Validation of a nonlinear wave decomposition method including shoaling for irregular waves

Ridder, Menno De; Bieman, Joost Den; Kramer, Jan

DOI
10.59490/jchs.2024.0037

Publication date
2024

Document Version
Final published version

Published in
Journal of Coastal and Hydraulic Structures

Citation (APA)
Ridder, M. D., Bieman, J. D., & Kramer, J. (2024). Validation of a nonlinear wave decomposition method including shoaling for irregular waves. *Journal of Coastal and Hydraulic Structures*, *4*, Article 37. https://doi.org/10.59490/jchs.2024.0037

JOURNAL OF COASTAL AND HYDRAULIC STRUCTURES

Vol. 4, 2024, 37

Validation of a nonlinear wave decomposition method including shoaling for irregular waves

Menno P. de Ridder[1], Joost P. den Bieman[2], Jan Kramer[3]

[1]Menno.deridder@deltares.nl, Deltares & Delft University of Technology, Delft, the Netherlands
[2]joost.denbieman@deltares.nl, Deltares, Delft, the Netherlands
[3]jan.kramer@deltares.nl, Deltares, Delft, the Netherlands

Research Article. **Submitted:** 25 June 2024. **Reviewed:** 1 August 2024. **Accepted** after double-anonymous review: 22 October 2024. **Published:** 2 December 2024

DOI: 10.59490/jchs.2024.0037

Cite as: "de Ridder, M., den Bieman, J., & Kramer, J. Validation of a nonlinear wave decomposition method including shoaling for irregular waves. *Journal of Coastal and Hydraulic Structures*. Retrieved from https://journals.open.tudelft.nl/jchs/article/view/7708".

This paper is part of the **Thematic Series** of selected papers on advances in physical modelling and measurement of Coastal Engineering issues, as presented on the Coastlab Conference in Delft in 2024.

Abstract

Decomposing the measured signals into incident and reflected signals is important when performing physical model experiments. Many methods exist to decompose a signal but limited studies focus on the effect of a sloping bed. In this paper, a nonlinear decomposition method is extended for a sloping bed by accounting for shoaling and phase transformation over a sloping bed with a simplified approach. Verification with linear synthetic signals shows that the error for the wave height is limited for intermediate water depth, but increases for shallow water depth with an error of up to 4%. Moreover, if the sloping bed is not considered in the decomposition, the wave height at the first wave gauge is overestimated in shallow water and underestimated in deep water. The numerical simulations show that a shoaling coefficient for the bound waves based on the water depth ratio with a power 1 is reasonably accurate for the sub-harmonics but not valid for higher harmonics. In addition, it is recommended to verify the shoaling of bound waves for a large range of test conditions. When applying the method both with and without the effects of a sloping bed in physical model experiments, the average relative differences for the wave height are 1 % with a maximum up to 4 %.

Keywords

Wave decomposition, Shoaling, Physical model experiments, Nonlinear waves

1 Introduction

Decomposing the measured wave signal into the incident and the reflected waves is important when performing physical or numerical experiments in a wave flume. Particularly, when a large reflection is expected, for example, from a breakwater, the measured signal can significantly deviate from the incident signal.

Different techniques exist to decompose a signal into incident and reflected signals. For 1DH wave flumes, a method based on co-located wave gauges (e.g. Nwogu, 1989, Sheremet et al., 2002) or multiple wave gauges (e.g. Eldrup and Lykke Andersen, 2019, Zelt and Skjelbreia, 1993, Mansard and Funke, 1980) is commonly applied. The latter is the focus

of this paper because the decomposition method based on multiple wave gauges was recently extended to be applicable to nonlinear irregular waves by including bound waves and amplitude dispersion (Eldrup and Lykke Andersen, 2019, Lin and Huang, 2004). A decomposition method based on multiple wave gauges is based on the phase difference between the different wave gauges, where the phase difference can be obtained from the linear dispersion relation. Lin and Huang (2004) derived a nonlinear decomposition method including the higher bound wave components for regular waves. Medina (2001) used a different approach for regular waves based on local time solutions to include nonlinear effects. Later Andersen and Eldrup (2007) extended the nonlinear decomposition method of Lin and Huang (2004) by adding the effects of amplitude dispersion with an iterative procedure. In Eldrup and Lykke Andersen (2019), the method was extended to irregular waves. Moreover, the practical requirements for the nonlinear wave decomposition methods were described in De Ridder et al. (2023) including a robust solution algorithm and the required number of wave gauges.

Most of the nonlinear wave decomposition methods are only applicable to a flat bed and will introduce an error when applied on a sloping foreshore, which is typically the case in physical model experiments. During most physical model experiments, one is interested in the wave conditions near the toe of the tested structure, and when a foreshore is present the wave gauges need to be placed on a sloping bed. An artificial flatbed could be constructed before the structure to place the wave gauges on a flatbed, but because a certain distance between the structure and the wave gauges is required (Klopman and Van der Meer, 1999), this would require significant space in the wave flume. It would therefore be desired to apply a decomposition method that is valid for a sloping bed.

Padilla and Alsina (2020) derived a general framework that included bound waves for a sloping bed but did not verify the framework with physical model experiments. In addition, Lykke Andersen and Eldrup (2021) presented a method for nonlinear waves over a sloping bed based on a nonlinear shoaling model, but this model is only applicable to regular waves.

Several decomposition methods are available but there is not yet a decomposition model for sloping foreshores for nonlinear irregular waves. In addition, it is also not fully known what the added value is of a decomposition method including bed slope effects for typical model experiments, and how this method affects the results. Therefore, in this paper, a nonlinear decomposition method for irregular waves is extended with the effects of a sloping bed with a simplified approach, and the effects of this method on typical wave parameters are studied. The objective of this paper is not to derive a method for a sloping foreshore, but rather to make a first step and demonstrate important elements of such a method.

2 Theory

The nonlinear wave decomposition method as described in Eldrup and Lykke Andersen (2019) with the solution algorithm as described in De Ridder et al. (2023) is extended to include the effect of a sloping foreshore. Before the theoretical background of the method including shoaling is given, the nonlinear method is briefly summarized. In essence, the following system of equations is solved for each frequency to decompose the signal without the effects of shoaling,

$$\mathrm{Z}\mathbf{a} = \boldsymbol{\zeta} \quad (1)$$

where Z is the phase-difference matrix, $\boldsymbol{a}$ a vector with the incident and reflected wave components and $\boldsymbol{\zeta}$ a vector with the observed complex amplitude. In matrix form, this equation is given by,

$$\begin{bmatrix} 1 & 1 \\ \dots & \dots \\ e^{-ik\beta_{in}x_{1N}} & e^{+ik\beta_{re}x_{1N}} \end{bmatrix} \begin{bmatrix} \hat{a}_{in,F} \\ \hat{a}_{re,B} \end{bmatrix} = \begin{bmatrix} \widehat{\zeta_1} \\ \dots \\ \widehat{\zeta_N} \end{bmatrix} \quad (2)$$

where k is the free wave number, β_{in} the amplitude dispersion factor for incident waves, β_{re} the amplitude dispersion factor for reflected wave, $\hat{a}_{in,F}$ the incident free complex wave amplitude, $\hat{a}_{re,F}$ the reflected free complex wave amplitude, ζ_j the measured complex wave amplitude at wave gauge j for $j=1 \dots N$ and x_{1J} the distance between wave gauge j and the first wave gauge. The amplitude dispersion factors are solved iteratively as proposed by Eldrup and Lykke Andersen (2019). To include the bound waves in the decomposition several regions are defined in the spectrum and depending on the region the following system of equations is solved instead of Equation 2,

$$\begin{bmatrix} 1 & 1 & 1 & 1 \\ e^{-ik\beta_{in}x_{12}} & e^{+ik\beta_{re}x_{12}} & e^{-ik_B\beta_{in}x_{12}} & e^{+ik_B\beta_{re}x_{12}} \\ \dots & \dots & \dots & \dots \\ e^{-ik\beta_{in}x_{1N}} & e^{+k\beta_{re}x_{1N}} & e^{-ik_B\beta_{in}x_{1N}} & e^{+ik_N\beta_{re}x_{1N}} \end{bmatrix} \begin{bmatrix} \hat{a}_{in,F} \\ \hat{a}_{re,F} \\ \hat{a}_{in,B} \\ \hat{a}_{re,B} \end{bmatrix} = \begin{bmatrix} \widehat{\zeta_1} \\ \dots \\ \widehat{\zeta_N} \end{bmatrix} \quad (3)$$

where k_B is the bound wave number, $\hat{a}_{in,B}$ the incident bound complex wave amplitude and $\hat{a}_{re,B}$ the reflected bound complex wave amplitude. Based on the peak (radial) frequency (ω_p) the following regions are defined in the spectrum:

- Region I: Sub-harmonic region ($\omega < 0.5\omega_p$). In addition to the free waves bound waves are present. The wave celerity of the bound waves is equal to the group velocity based on the peak frequency. The bound wave number is given by: $k_B = \omega c_g(\omega_p, h)$
- Region II: Primary region ($0.5\omega_p < \omega < 1.5\omega_p$). Only primary free waves exist. Equation 2 is solved.
- Region III: Super-harmonic region ($1.5\omega_p < \omega < 2.5\omega_p$). In addition to the free waves bound waves are present. The wave celerity of the bound waves is equal to the celerity of the corresponding primary wave. The bound wave number is given by: $k_B = nk(\frac{\omega}{n}, h)$ where n is equal to 2
- Region IV: Super-harmonic region ($2.5\omega_p < \omega < 3.5\omega_p$). This region is identical to Region III, but n is equal to 3.
- Region V: Super-harmonic region ($3.5\omega_p < \omega < 4.5\omega_p$). This region is identical to Region III, but n is equal to 4.
- Region VI: Super-harmonic region ($4.5\ \omega_p < \omega$). In the tail of the spectrum, only free waves are present. Equation 2 is solved without the effects of amplitude dispersion.

Moreover, when the sensitivity to noise to too large, the system of equations is reduced to 2 or 3 equations as described in De Ridder et al. (2023) by ignoring the bound reflected waves or ignoring the incident free waves and the bound reflected waves. The sensitivity to noise is evaluated based on the condition number of the phase difference matrix *Z*. When this condition number is larger than a prescribed maximum, the system of equation is simplified. First, the bound reflected wave components are removed when the condition number is too high (3 equations). When the condition number is still larger than the prescribed maximum, the system of equations is further simplified by removing the incident free waves (2 equations). This decomposition method, without the effects of a sloping bed, is called the Reference method in this study.

The system of equations is slightly adjusted to include the effects of a sloping bed. First, a spatially varying phase, $\theta(x)$, is computed at position x with,

$$\theta(x) = \int_{x_1}^{x_j} k(x)dx \quad (4)$$

where $k(x)$ is the wave number, x_1 is the first wave gauge position and xj is the wave gauge position at location j. This phase shift, $\theta(x)$, replaces the bound or free wave number times the wave gauge spacing (kx_{1N}) in Equation 2. Only a spatially varying phase is implemented for the free components because the phase transformation of the bound waves is not easily available because the phase of the bound wave will start lagging behind the primary waves. In Van Dongeren et al., (2007) an iterative method was proposed to obtain the phase of the bound long wave, but this method does not distinguish between bound and free waves for the same direction (incident waves were assumed to be bound and reflected waves were assumed to be free). It can also be argued that for the low-frequency waves, the effect of the changing phase is limited because mostly the wave gauge array is much shorter than the wavelength.

The second adjustment includes a shoaling coefficient in Equation 1 to correct for the energy transformation over the slope. For the free components linear shoaling is given by,

$$K_{lin} = \frac{c_{g,0}}{c_{g,1}} \quad (5)$$

where $c_{g,0}$ is the group velocity at the first wave gauge and $c_{g,1}$ is the group velocity at one of the other wave gauges. Equation 3 cannot be used for the bound components because the bound waves do not shoal in the same way as free

waves (Van Dongeren et al., 2007). Padilla and Alsina (2020), therefore suggest using the following shoaling coefficient for the bound waves,

$$K_{bnd} = \left(\frac{h_0}{h_1}\right)^{\alpha} \qquad (6)$$

where h_0 is the water depth at the first wave gauge and h_1 is the water depth at the considered wave gauge. An α of 1 is assumed in this study, but sensitivity should be verified. This approach oversimplifies the bound wave shoaling significantly. For example, the energy transfer from the primary waves to the bound waves is not accounted for in this method, which would result in a decrease of energy in the primary part of the spectrum. Secondly, it is known that the shoaling of bound waves is also related to the bed slope (e.g. Battjes et al., 2004), but only the water depth difference (and not directly the slope) is included in the current approach. Since no fast approach exists to obtain a bound wave shoaling coefficient, this method is implemented and verified in this manuscript.

Thus the system of equations including shoaling for the regions with bound waves is given by,

$$\begin{bmatrix} 1 & 1 & 1 & 1 \\ K_{lin}e^{-i\beta_{in}\theta_{12}} & K_{lin}e^{+i\beta_{re}\theta_{12}} & K_{bnd}e^{-ik_B\beta_{in}x_{12}} & K_{bnd}e^{+ik_B\beta_{re}x_{12}} \\ \dots & \dots & \dots & \dots \\ K_{lin}e^{-i\beta_{in}\theta_{1N}} & K_{lin}e^{+\beta_{re}\theta_{1N}} & K_{bnd}e^{-ik_B\beta_{in}x_{1N}} & K_{bnd}e^{+ik_N\beta_{re}x_{1N}} \end{bmatrix} \begin{bmatrix} \hat{a}_{in,F} \\ \hat{a}_{re,F} \\ \hat{a}_{in,B} \\ \hat{a}_{re,B} \end{bmatrix} = \begin{bmatrix} \widehat{\zeta_1} \\ \dots \\ \widehat{\zeta_N} \end{bmatrix} \qquad (7)$$

The phase, θ_{1N}, is obtained through numerical integration of equation 2. For region II (primary waves) Equation 5 is solved but without the bound wave components.

One of the processes that is still not accounted for is wave breaking, which makes this method only applicable to non-breaking wave conditions. Both depth-induced and breaking based on steepness should not occur. When the method is applied for these conditions the error will be significant because the actual wave height decreases, but the wave height obtained with the decomposition method will increase within the wave gauge array.

3 Verification

To check the implementation and its effect, the method with and without the effects of a sloping bed (reference and including sloping bed) is applied to synthetic (linear) irregular wave signals and signals obtained from a numerical model.

3.1 Synthetic wave signals

The synthetic signals with a duration of 1200 s are created based on wave components from a JONSWAP spectrum. The time series is created based on the Fast Fourier Transform of the Fourier components. A time step of 0.01 s is applied which means that the Nyquist frequency is 50 Hz. For every frequency, the amplitude (A) of the Fourier components is obtained from the JONSWAP energy density function. Random phases (φ) are applied for every component. Each wave component is translated to the locations of the wave gauges including the effect of shoaling and the spatially varying wave number according to,

$$\hat{a} = K_{lin}\frac{A}{2}e^{i(\int k(x)dx+\phi)} \qquad (8)$$

where $k(x)$ is the wavenumber as a function of the location and K_{lin} is the linear shoaling coefficient.

Six wave gauges are applied (Δ_{x12} = 0.45m, Δ_{x23}=1.5m, Δ_{x34}=0.45m, Δ_{x45}=0.37m, Δ_{x56}=0.15 m). The second-order bound waves are not included to only show the effect for linear waves making it not possible to validate the bound wave shoaling formulation. The synthetic wave signals are constructed for a 1:20 slope with an initial water depth of 0.6 m and 0.4 m. Moreover, three different wave conditions are verified. A signal for a peak frequency of 0.4 Hz, 0.66 Hz, and 1Hz with a wave height of 0.05 m. These conditions were created because they capture both deep and shallow water conditions. A small amplitude is applied because we want to verify the effect of linear wave conditions.

For each condition, the target incident wave height is compared to the incident wave height obtained with both methods (See Figure 1). It can be observed that when considering the first wave gauge, the method that does not account

for a sloping bed overestimates the wave height in shallow water and underestimates the wave height in deep water (Panel A). The opposite is true for the last wave gauge (Panel B). This effect is caused by the average water depth which is applied for the Reference method. By assuming an average water depth, the bias in the wave height for the first and last wave gauges is different. The bias is approximately zero for a wave gauge in the center of the set. The different behaviors for deep and shallow water can be explained based on the shoaling coefficient. In shallow water, the shoaling coefficient is larger than 1 increasing the wave amplitude, whereas the shoaling coefficient in deep water is lower than 1 resulting in a decrease of the wave amplitude.

These results show that the effect of shoaling in terms of wave height is minimal for most of the wave conditions. Only for extremely shallow water conditions (h/L<0.15), the error goes up to 4 % when bed slope effects are not included.

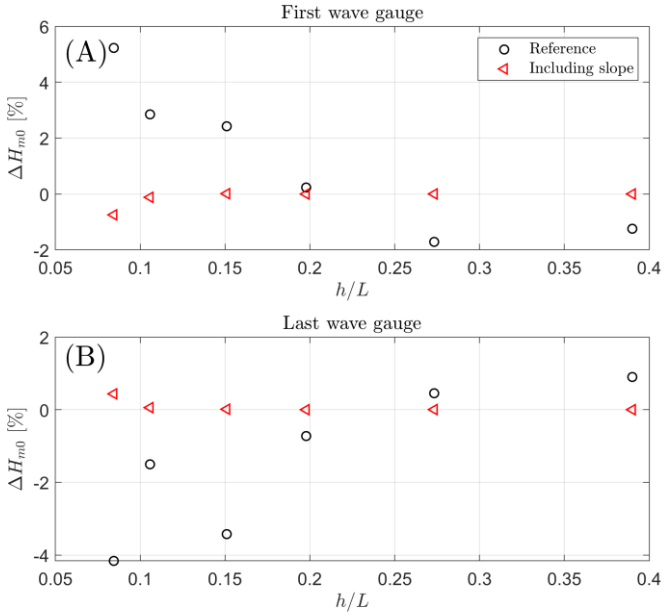

Figure 1: Difference in significant wave height for the first (Panel A) and last (Panel B) wave gauge for various wave conditions. The black points are obtained from the Reference method and the red points are obtained from the method including a sloping foreshore.

To demonstrate the effect of the incident wave spectrum, linear shoaling coefficients for the different wave gauges, phases for different locations, and spectrum of the residual term are shown in Figure 2 for the wave conditions with a peak frequency of 0.66 Hz and a water depth of 0.4 m (for the first wave gauge). In this figure, it can be seen that the incident spectral shape changes slightly between the two methods. The decomposition method without shoaling has too much energy around the peak, whereas the method with a sloping bed matched the target spectrum at the first wave gauge. This difference is mainly caused by the shoaling of waves, which is demonstrated by the linear shoaling coefficient (Panel B of Figure 1). Even though the shoaling coefficient is small (~1.02) between the wave gauges, it results in a non-constant distribution of the energy between the wave gauges. The phase shift is demonstrated in Panel B for the wave gauges. Especially a large phase error is introduced with a sloping bed for higher frequencies where the wavelength is relatively short compared to the wave gauge distance. Thus, in contrast to the shoaling coefficient, the phase is important for higher frequencies whereas shoaling is mainly dominant for the lower frequencies. In the last panel the spectrum of the residual signal after the decomposition is shown. This result shows that a method without shoaling has a larger error around the peak frequency. This error is lower with the method including shoaling.

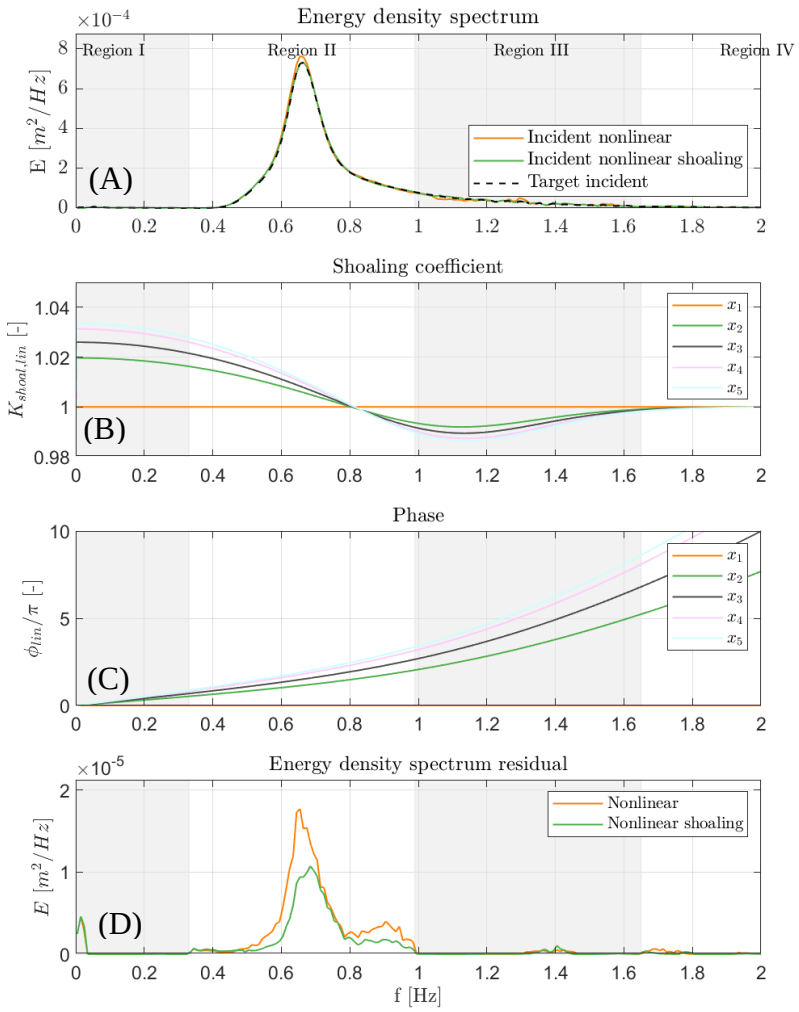

Figure 2: Panel A shows the incident wave spectrum obtained from the target signal, the decomposition method with bed slope effects (Nonlinear shoaling), and the decomposition method without bed slope effects (Nonlinear). Panel B shows the linear shoaling coefficient for the different wave gauges. The phase is shown in Panel C for the different locations. Panel D shows the spectrum of the residual term after decomposition. The results are shown for the condition with a peak frequency of 0.66 Hz and a water depth of 0.4 m.

3.2 Numerical simulations

To verify the bound wave shoaling, numerical simulations were conducted. The simulations are applied with the non-hydrostatic model XBeach. This model is applicable for modeling bulk wave statistics, spectral shape, and second-order statistics (de Ridder et al., 2019).

Waves from a JONSWAP spectrum with second-order waves are forced at the boundary at a depth of 1 m. At a distance of 25 m from the boundary a slope of 1:50 starts with a distance of 25 m. After this slope, a constant bed level of -0.5 m is present with a length of 100 m (see Figure 3). To absorb the waves a 75 m sponge layer is used at the back side of the model. This means that there are no reflections in the model and the incident wave signal is equal to the signal obtained from XBeach (target signal). The model is discretized with a spatially varying resolution of 40 points per wavelength based on a period of 2 s with a minimum grid resolution of 0.01 m. The simulation is computed for 3600 s. Three different wave conditions are verified (see Table *1*).

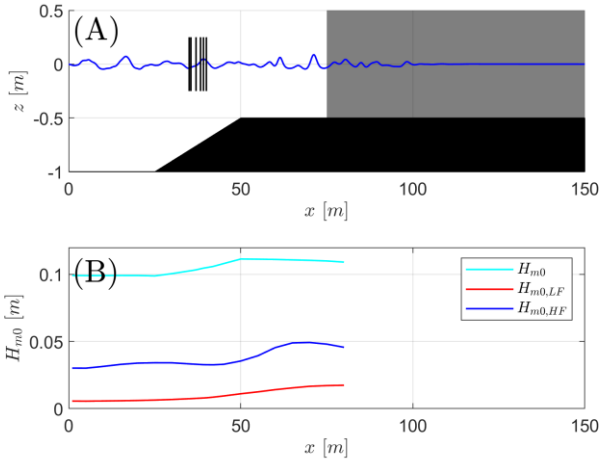

Figure 3: Domain of the numerical model (Panel A) and wave transformation of the wave heights (Panel B). Both the total wave height (cyan), low-frequency wave height (red), and high-frequency wave height (blue) are shown. The relaxation zone is shown in grey.

The results for test A1 are shown in Figure 4. In this figure, the relative wave height (normalized with the wave height at the last wave gauge from the numerical model) for different wave gauges and frequency ranges is shown. Both the relative energy for the total wave height ($H_{m0}/H_{m0,target,last}$), relative low-frequency wave height for frequencies lower than $f_p/2$ ($H_{m0,LF}/H_{m0,LF,model,last}$) and the relative energy for frequencies within the super-harmonic region ($H_{m0,HF}/H_{m0,HF,target,last}$ for frequencies between $f_p+f_p/2$ and f_p+f_p) are considered. This result shows that the assumed shoaling coefficient performs reasonably well, especially for the wave height and low-frequency wave height. When considering the energy in the super-harmonic region, shoaling is overestimated resulting in too much energy at the last wave gauge.

In Table *1*, the error with the target wave height obtained from the numerical model is shown. This result shows that the findings for condition A1 also hold for the other wave conditions. The shoaling of the sub-harmonic is accurately captured, but the error with the method including bed slope effects is larger for the super-harmonic. The shoaling of the super-harmonics is overestimated with the current formulation for the three conditions showing that it is not possible to apply a generic shoaling coefficient for the bound waves. Although the shoaling of the super harmonics is overestimated, the (total) wave height is better captured with the method including bed slope effects.

Table 1: Result for the three different wave conditions. The relative differences between the two methods and the target value are computed for the last wave gauge.

TestID	H_{m0} [m]	T_p [s]	Method	$(H_{m0,target}-H_{m0})/H_{m0,target}$	$(H_{m0,LF,target}-H_{m0,LF})/H_{m0,LF,target}$	$(H_{m0,HF,target}-H_{m0,HF})/H_{m0,HF,target}$
A1	0.1	4	Reference:	0.0100	0.150	-0.001
			Including slope:	0.0001	0.088	-2.7
A2	0.1	3.3	Reference:	0.0028	0.120	-0.14
			Including slope:	0.0001	0.077	-3.53
A3	0.1	1.53	Reference:	0.0109	0.121	-0.056
			Including slope:	-0.0055	0.066	-2.59

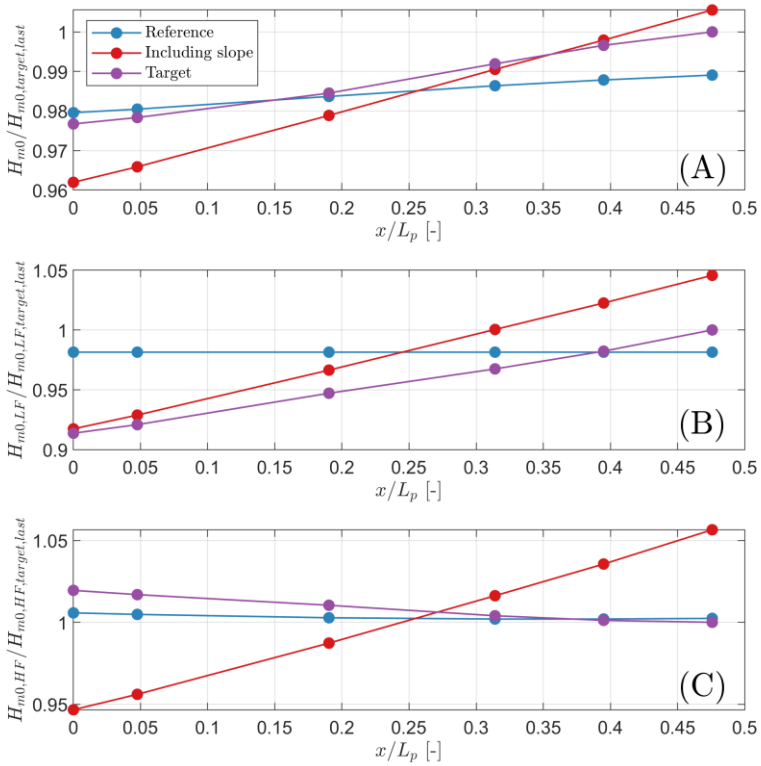

Figure 4: Validation of the significant wave height (Panel A), low-frequency wave height (Panel B), and high-frequency wave height(Panel C) for test A1. The results for the Reference decomposition methods (blue), decomposition method including slope effects (red), and the target values obtained with the numerical model (purple). The target values are defined as the wave parameter obtained with the numerical model (Target) for the last wave gauge.

4 Physical model experiments

4.1 Model setup

The decomposition with and without the effects of a sloping bed were both applied to a set of physical model experiments (See Table 2). A 1:50 slope was placed in the flume until a height of 0.327 m. The start of the foreshore is located 23.17 m from the waveboard. A typical rubble mound breakwater (armour layer 0.066 m; height 0.773m) with a 1:2 foreshore is located at the end of the foreshore (x = 39.17 m) to obtain a signal with reflections. The wave gauge array on the foreshore is located at 32.176 m. A complete overview of the experiments is given in de Ridder et al., (2023). Waves were forced with a piston type of wave board including second-order effects and active reflection compensation. Seven wave gauges were used to decompose the measured signal into incident and reflected signals for both methods which are located at 32.176, 33.026, 33.186, 33.661, 34.26, 34.787, and 35.17 m. The mean water depth over the wave gauge array is applied for the Reference method.

A large range of wave conditions was tested with variations in the offshore water depth (0.6, 0.7, and 0.8 m), wave steepness (1 – 4%), and peak enhancement factor. Not all the experiments shown in Ridder et al., (2023) were used, because only tests with a relative water depth (H_{m0}/d) smaller than 0.4 in combination with a low breaker parameter ($\zeta \leq 0.1$) are considered because no wave breaking can be assumed for these conditions.

Table 2: Overview of physical model tests used to verify the decomposition methods. In the table, both the target wave height (H_{m0}), peak period (T_p), and peak enhancement factor (γ) are shown. Also, the slope and the water depth at the start and end of the wave gauge array are shown (d_1 and d_2). The last column shows the observed breaker parameter.

TestID	H_{m0} [m]	T_p [s]	d_1 [m]	d_2 [m]	Slope	γ	$\zeta_{m-1,0}$
A102	0.15	2.17	0.42	0.36	1/50	3.3	0.07
A103	0.15	1.53	0.42	0.36	1/50	3.3	0.05
A103_hi	0.2	1.53	0.42	0.36	1/50	3.3	0.05
A113	0.15	1.53	0.42	0.36	1/50	5	0.05
A201	0.15	3.43	0.52	0.46	1/50	3.3	0.10
A202	0.15	2.17	0.52	0.46	1/50	3.3	0.07
A203	0.15	1.53	0.52	0.46	1/50	3.3	0.05
A223	0.15	1.53	0.52	0.46	1/50	5	0.05
A301	0.15	3.43	0.62	0.56	1/50	3.3	0.10
A302	0.15	2.17	0.62	0.56	1/50	3.3	0.07
A303	0.15	1.53	0.62	0.56	1/50	3.3	0.05
A303_hi	0.20	1.53	0.62	0.56	1/50	3.3	0.05
A303_lo	0.05	1.53	0.62	0.56	1/50	3.3	0.05
A303_lo	0.05	3.43	0.62	0.56	1/50	3.3	0.10
A323	0.15	1.53	0.62	0.56	1/50	5	0.05
A321	0.15	3.43	0.62	0.56	1/50	3.3	0.10

4.2 Results

All the tests are analyzed with the method including bed slope effects and without bed slope effects. For one of the tests, the results are shown in Figure 5. Panel A shows the incident time series obtained with both methods for test A103 and Panel B the incident spectrum. Also, the difference between the two methods is shown. The largest differences between both methods are observed around the peak frequency. In addition, significant differences are observed at the lower frequencies and higher frequencies. However, considering the numerical simulation it was observed that only the shoaling of the low-frequencies was correctly captured. To identify the effect of both methods on the error signal after the decomposition ($\eta_{error}=\eta_{In}+\eta_{Re}-\eta_{observed}$), the spectrum of the error signal is shown in Panel B of Figure 5 for the first and last wave gauge. This figure shows that the error signal is lower around the peak frequency, but not significantly lower at the higher and in this case also not significantly lower at the lower frequencies for both the first and the last wave gauge. This suggests that only the energy around the peak frequency is well captured with the model including bed slope effects.

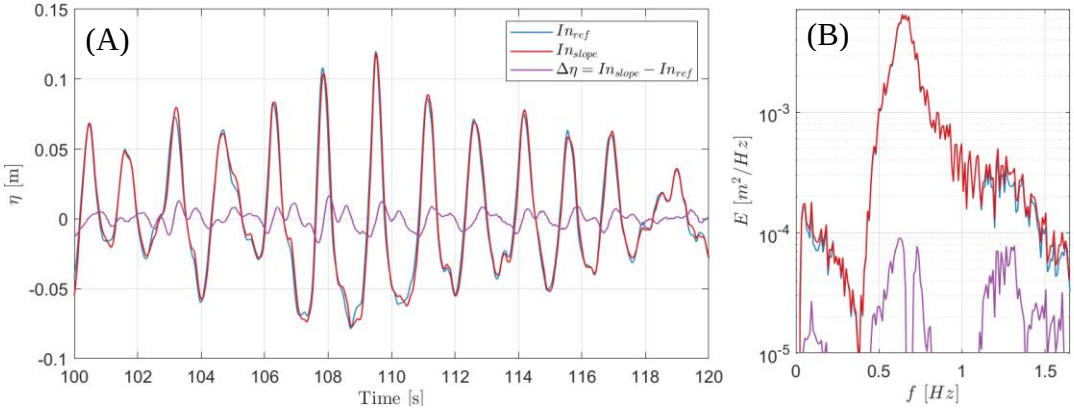

Figure 5: Time series (Panel A) and spectrum (Panel B) of incident time series at the last wave gauge of the wave gauge array. Results are shown for test A103

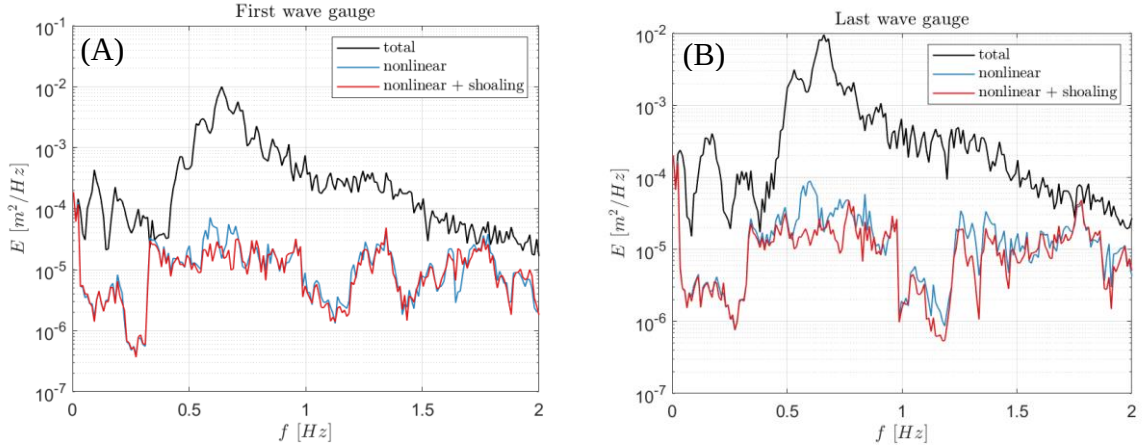

Figure 6: Observed signal for the first (Panel A) and last wave gauge (Panel B). The spectrum of the error signal is shown in blue and red for respectively the Reference method and the method including slope effects. The results are shown for test A103.

The differences between both methods are shown for the first and last wave gauge of the wave gauge array in Figure 7. The first and last wave gauges are analyzed because the differences between the Reference method and the method including slope effects are largest for the first and last wave gauge because the mean water depth is applied in the Reference method. Moreover, mostly in practical applications, the last wave gauges will be used because it is the closest to the structure. The comparison of the relative error between both methods shows that for the first wave gauge, the method including bed slope effects results in a higher incident wave height compared to a method with bed slope effects (see Panel A). On the other hand, a lower incident wave height is found for the last wave gauge using the method, including bed slope effects. The largest deviation found in the conditions is 4% but the mean is approximately 1%.

A similar result is found for the reflection coefficient (Panel B). Also here a different effect is found for the first and the last wave gauge of the set. The first wave gauge results in a higher reflection coefficient when the method including shoaling is applied and a lower reflection coefficient for the last wave gauge.

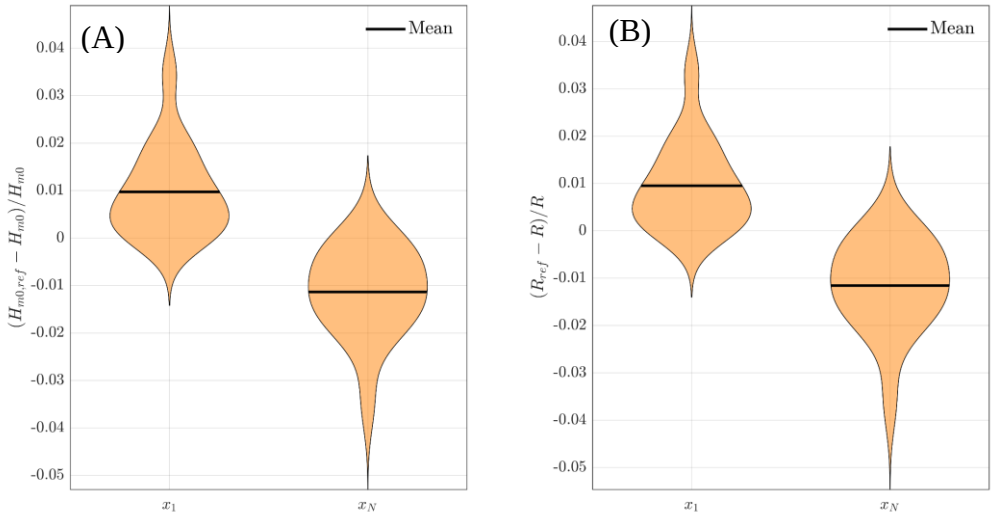

Figure 7: Violin plot of the relative error in the incident wave height (Panel A) and reflection coefficients (Panel B). The results for both the first (x_1) and last wave gauges are shown (x_n). The mean of all the points is shown with a black line.

5 Discussion

The effects of a sloping bed on the decomposition method are shown based on linear synthetic signals, numerical simulation, and physical experiments. However, the model is only validated for a limited set of wave conditions. The validation based on linear synthetic signals indicates the effects of a sloping bed for various water depths but does not show the validity for nonlinear effects. The validation based on numerical simulations does show the accuracy of nonlinear shoaling effects, but a limited set of geometries and wave conditions is verified in this study. Although only three conditions are verified, it can already be observed that the shoaling of super harmonics is not accurately captured with the current approach. The accuracy of the low-frequency shoaling model is reasonably accurate but it is recommended to also verify the effects for other foreshore slopes and different wave conditions.

The decomposition model applied in this study is based on several assumptions. One of the assumptions is that the phase transformation of the bound waves is not adjusted in contrast to the free components where the phase transformation is accounted for. In Padilla and Alsina (2020) a framework with the phase transformation for the bound waves is presented but it does not account for the phase transformation over a sloping bed. This study chooses to ignore this effect to keep the approach simple and because the phase transformation of bound waves is not well understood. When considering the low-frequency waves the validation based on numerical simulations reveals that the current approach is, although the simplification, better than the Reference method. For the higher frequencies, a different approach is needed.

Another simplification is the linear shoaling coefficient. In Eldrup and Lykke Andersen (2020), the effects of nonlinear shoaling are demonstrated with a numerical model for regular waves. These results show that the (nonlinear) shoaling coefficient is also dependent on the wave height. For regular waves, this effect can relatively easily be included but it becomes more complicated for irregular waves, especially because other aspects also play a role (e.g. wave interactions between wave components).

Both the applicability range (range of wave conditions for the method is applicable) and the added value compared to the Reference model are important for the actual use of a decomposition method for a sloping bed. The results show that the effects of shoaling can be significant (up to 4%) but the error will increase when it is applied outside the applicability range (not shown in this study). When waves are breaking instead of shoaling the effects of shoaling in the decomposition method will increase the error. This means that there is a small window where the method has added value and improves the decomposition. The largest shoaling effect is found just before the water depth where waves break. One has to be

careful when applying a method including shoaling, especially when the wave gauges are located in relatively shallow water.

Thus, a decomposition method with the effects of a sloping foreshore is mainly preferred when the transformation of the wave height is large but the waves are not breaking. This can be expected for large wave gauge arrays over a sloping bed, relatively steep slopes, or wave conditions with long waves. For these conditions, the wave height will transform significantly within the wave gauge array. Furthermore, it could also be preferred when only the low-frequency part of the wave spectra is desired. These long waves start to break only for very mildly sloping slopes but can transform significantly over a sloping bed.

To obtain a more accurate decomposition, it could be argued that a numerical model would be a better approach to obtain the incident waves over a sloping bed. Nowadays the computation time of phase-resolving models is sufficient to apply it for the computation of incident waves. Instead of decomposing a wave signal obtained from a physical wave flume, the wave flume could be modeled with a numerical model to estimate the incident waves. For example, with a sponge layer of absorbing boundary at the onshore boundary of the model. In this way, all the relevant nonlinear effects are included in the incident signal. However, this approach is only useful when only the incident waves are required. When also the reflection coefficient needs to be known, wave decomposition methods are needed. To obtain a fully nonlinear method for a sloping bed hybrid method based on numerical simulations could be a solution.

6 Conclusions

A nonlinear decomposition method for nonlinear waves is extended to include the effects of a sloping bed with a simplified approach. The method is adjusted by including a spatially varying phase and a shoaling coefficient for both the free and bound waves. Verification with linear synthetic signals shows that the effect on the wave height is limited for intermediate water depth, but increases for shallow water depth with an error of up to 4% for the wave height when not accounting for a sloping bed. Moreover, when not accounted for a sloping bed the wave height at the first wave gauge is overestimated in shallow water and underestimated in deep water. The opposite behaviour is present for the last wave gauge of the array where the method without bed slope effects underestimated the wave height.

The shoaling of bound waves is verified using three numerical simulations. The results suggest that a shoaling coefficient based on the water depth ratio with a power of 1 is not applicable for both the sub-harmonics and the super-harmonics. Considering the sub-harmonics the results seem to improve the decomposition, but verifying this assumption for a large range of test conditions is recommended. Conversely, the energy at the higher frequencies did not improve with the current formulation, showing an area for improvement in future work.

The results obtained from a decomposition method with and without bed slope effects are compared for a set of typical physical model experiments. These results show that the differences in wave height are relatively small with the mean relative deviation lower than 1 % and only a few tests with a relative deviation of 4 %.

Acknowledgments

Funding

The support by Deltares via Deltares' Strategic Research Program Knowledge Basis Facilities is acknowledged.

Author contributions (CRediT)

M. P. de Ridder: Conceptualization, Formal Analysis, Investigation, Methodology, Software, Validation, Visualization and Writing – original draft. J. P. den Bieman: Writing – review & editing and Software. J. Kramer: Writing – review & editing, Project administration and Software.

Data access statement

The data (wave parameters) used in the study will be made available on request.

Declaration of interests

The authors report no conflict of interest.

References

Andersen, T. L., Eldrup, M. R., & Frigaard, P. (2017). Estimation of incident and reflected components in highly nonlinear regular waves. *Coastal Engineering*, *119*, 51-64. https://doi.org/10.1016/j.coastaleng.2016.08.013

Andersen, T. L., & Eldrup, M. R. (2021). Estimation of incident and reflected components in nonlinear regular waves over sloping foreshores. *Coastal Engineering*, *169*, 103974. https://doi.org/10.1016/j.coastaleng.2021.103974

Battjes, J. A., Bakkenes, H. J., Janssen, T. T., & van Dongeren, A. R. (2004). Shoaling of subharmonic gravity waves. *Journal of Geophysical Research: Oceans*, *109*(C2). https://doi.org/10.1029/2003JC001863

de Ridder, M. P., Kramer, J., den Bieman, J. P., & Wenneker, I. (2023). Validation and practical application of nonlinear wave decomposition methods for irregular waves. *Coastal Engineering*, *183*, 104311. https://doi.org/10.1016/j.coastaleng.2023.104311

de Ridder, M. P., Smit, P. B., van Dongeren, A. R., McCall, R. T., Nederhoff, K., & Reniers, A. J. (2021). Efficient two-layer non-hydrostatic wave model with accurate dispersive behaviour. *Coastal Engineering*, *164*, 103808. https://doi.org/10.1016/j.coastaleng.2020.103808

Eldrup, M. R., & Lykke Andersen, T. (2020). Numerical study on regular wave shoaling, de-shoaling and decomposition of free/bound waves on gentle and steep foreshores. *Journal of Marine Science and Engineering*, *8*(5), 334. https://doi.org/10.3390/jmse8050334

Van Dongeren, A. R. J. A., Battjes, J., Janssen, T., Van Noorloos, J., Steenhauer, K., Steenbergen, G., & Reniers, A. J. H. M. (2007). Shoaling and shoreline dissipation of low-frequency waves. *Journal of Geophysical Research: Oceans*, *112*(C2). https://doi.org/10.1029/2006JC003701

Eldrup, M.R., & Lykke Andersen, T. (2019). Estimation of incident and reflected wave trains in highly nonlinear two-dimensional irregular waves. *Journal of Waterway, Port, Coastal, and Ocean Engineering*, *145*(1), 04018038. https://doi.org/10.1061/(ASCE)WW.1943-5460.0000497

Nwogu, O. (1989). Maximum entropy estimation of directional wave spectra from an array of wave probes. *Applied Ocean Research*, *11*(4), 176-182. https://doi.org/10.1016/0141-1187(89)90016-3

Mansard, E. P., & Funke, E. R. (1980). The measurement of incident and reflected spectra using a least squares method. *Coastal Engineering*, 154-172. https://doi.org/10.1061/9780872622647.008

Medina, J. R. (2001). Estimation of incident and reflected waves using simulated annealing. *Journal of waterway, port, coastal, and ocean engineering*, *127*(4), 213-221. https://doi.org/10.1061/(ASCE)0733-950X(2001)127:4(213)

Padilla, E. M., & Alsina, J. M. (2020). A general framework for wave separation in the frequency domain. *Coastal Engineering*, *158*, 103686. https://doi.org/10.1016/j.coastaleng.2020.103686

Lin, C. Y., & Huang, C. J. (2004). Decomposition of incident and reflected higher harmonic waves using four wave gauges. *Coastal Engineering*, *51*(5-6), 395-406. https://doi.org/10.1016/j.coastaleng.2004.04.004

Sheremet, A., Guza, R. T., Elgar, S., & Herbers, T. H. C. (2002). Observations of nearshore infragravity waves: Seaward and shoreward propagating components. *Journal of Geophysical Research: Oceans*, *107*(C8), 10-1. https://doi.org/10.1029/2001JC000970

Klopman, G., & Meer, J. W. V. D. (1999). Random wave measurements in front of reflective structures. *Journal of waterway, port, coastal, and ocean engineering*, *125(1)*, 39-45. https://doi.org/10.1061/(ASCE)0733-950X(1999)125:1(39)

Zelt, J. A., & Skjelbreia, J. E. (1993). Estimating incident and reflected wave fields using an arbitrary number of wave gauges. *Coastal Engineering*, 777-789. https://doi.org/10.1061/9780872629332.058